INTERNATIONAL JOURNAL OF FLUID POWER, 2018
VOL. 19, NO. 1, 14–26
https://doi.org/10.1080/14399776.2017.1366245

Taylor & Francis
Taylor & Francis Group

Compensation of a hydraulic pipeline resonance by fluid–structure interaction

Gudrun Mikota[a], Rainer Haas[b] and Evgeny Lukachev[a]

[a]Institute of Machine Design and Hydraulic Drives, Johannes Kepler University Linz, Linz, Austria; [b]Linz Center of Mechatronics GmbH, Linz, Austria

ABSTRACT

For a pipeline between a valve block and a cylinder, the second hydraulic resonance is compensated by adding an appropriate mass in the most flexible part of the pipeline structure. The second maximum in the magnitude of measured pressure can thus be reduced to 65%. Frequency response functions between flow rate excitation and pressure as well as velocity response are calculated from a plane analytical model, including junction coupling. Results are validated against measurements in configurations with and without additional mass and with different layers of rubber in between. Calculated pressure responses clearly reproduce the measured compensation effect, and the model also provides a rough approximation of structural vibrations.

ARTICLE HISTORY
Received 24 May 2017
Accepted 7 August 2017

KEYWORDS
Pipeline dynamics; hydraulic behaviour; axial tension; bending; coupling; vibration compensation

1. Introduction

The frequency response between hydraulic states of a pipeline can be influenced by structural vibrations. In fluid power systems, this influence has been observed to increase with the order of the pipeline resonance. Substantial changes in dynamic behaviour include the possibility of vibration compensation, which sometimes occurs by chance for a higher order hydraulic resonance. In this paper, a pipeline structure is modified in such a way as to compensate the second hydraulic pipeline resonance peak.

The compensation of pressure pulsations in hydraulic systems is widely realised by λ/4- or Helmholtz type resonators, which were extensively discussed by Ingard (1953). The inconvenient size of such devices motivated the development of compact vibration compensators for hydraulic systems (Mikota 2002), and, in particular, the invention of a vibration compensator featuring a hydraulic spring (Mikota and Reiter 2003). This compensator includes a lumped mechanical mass which oscillates against the compressibility of a cavity connected to the fluid side of the hydraulic system.

Fluid–structure interaction in pipeline systems was studied by Lavooij and Tijsseling (1991), and three different coupling mechanisms were identified. Junction coupling originates from unbalanced pressure forces which cause a structural motion. Poisson coupling describes the axial movement of the pipeline structure due to radial compliance under pressure. Friction coupling is caused by fluid friction, and is generally considered as weak. Liu and Li (2011), Liu *et al.* (2013), and Xu *et al.* (2014) proposed transfer matrix methods for the vibration analysis of fluid–structure interaction in pipeline systems. These methods consider both junction and Poisson coupling; friction coupling is neglected, and, moreover, fluid friction is not taken into account in the hydraulic behaviour of the system. Transfer matrix methods aim at a relationship between state vectors that contain both motions and forcing functions; the inclusion of boundaries, excitation and constraints was treated by Xu *et al.* (2014).

A different view on fluid–structure interaction was taken by modal methods. Finite element modal analyses of fluid-filled pipelines were described by Li *et al.* (2011) and Makaryants *et al.* (2015); modal tests from a structural viewpoint were reported by Yigang *et al.* (1987) and Nurkkala *et al.* (2004). The experimental modal analysis of fluid dynamics in hydraulic pipeline systems was enabled by theoretical foundations from Mikota (2013) and can be extended to fluid–structure interaction systems considering the theory of vibro-acoustical modal analysis (Wyckaert *et al.* 1996). A modal test of a bent hydraulic pipeline in a fluid power system was carried out by Mikota *et al.* (2016a). This pipeline was investigated further by simple fluid–structure interaction models (Mikota *et al.* 2016b), and it was predicted that the second hydraulic resonance could be compensated by adding a mass at the pipeline bend. However, an experimental proof of this prediction and a more accurate fluid–structure interaction model were still missing.

In this paper, the test stand resembles the set-up from Mikota *et al.* (2016a, 2016b). The compensation of the second hydraulic pipeline resonance is realised in an experiment. In contrast to (Mikota and Reiter

CONTACT Gudrun Mikota gudrun.mikota@jku.at

2003), this is done by mechanical measures from outside; an appropriate mass is added in a suitable position of the pipeline. Various layers of rubber provide different amounts of damping between the pipeline and the additional mass. Experiments are supplemented by a fluid–structure interaction model that is restricted to junction coupling. A frequency response matrix is assembled which links flow rate and force input with pressure and velocity output in five system nodes and accounts for hydraulic behaviour as well as axial tension and bending of the pipeline. Compared to the methods from Liu and Li (2011), Liu *et al.* (2013), and Xu *et al.* (2014), this system model includes frequency-dependent friction. It readily incorporates lumped parameter components in the system nodes, and constraints can be approximated by an appropriate choice of such components. Compared to the model from Mikota *et al.* (2016b), a complete plane structural description of the pipeline is included; model parameters are determined more precisely, and a large number of structural resonances are taken into account. The model is validated by comparing measured and calculated frequency response functions in all configurations of the system.

2. Experimental set-up

The pipeline that shall be studied is part of a cylinder drive as shown in Figure 1. It leads from a valve block to a hydraulic cylinder and includes two 90° bends. Near the first bend, the pipeline is supported by a pillar. A supply pressure of 20 MPa on the ring side of the cylinder is balanced by an operating pressure of 6.5 MPa in the pipeline. The valve block contains four 2/2 way fast switching valves which can connect the pipeline with supply or tank. Experiments are controlled by a 2 ms flow rate pulse through one of the two supply sided valves. Pressure sensors are mounted at the valve block and both pipeline bends. The additional mass consists of three large discs and a tuning mass that is attached by a magnet. The discs can be screwed onto the fitting at the first pipeline bend. This configuration is shown in Figure 1; Figure 2 displays an optional layer of rubber between the pipeline and the additional mass.

Apart from the pillar, all vibrating beams are situated in the inclined plane spanned by the pipeline axis; the pipeline is separated from the pillar by a layer of rubber. An inclusion of the pillar would require a three-dimensional model as well as an identification of rubber stiffness and damping, which is outside the scope of this paper. Compared to the pipeline walls, the pillar in series with the rubber seems more compliant. It is therefore assumed that the influence of the pillar may be neglected; the validity of this assumption will be assessed by measurements in Sections 4 and 5. As an approximation, a plane model is used, which is described by the schematic in Figure 3. Nodes 1–5 are introduced to subdivide the model. The flow rate pulse enters the pipeline in node 1 and is reconstructed from a valve spool position measurement. Hydraulic pressure is measured in nodes 1–3; structural accelerations in three spatial directions are measured in node 2. For simplicity, the model terminates at the hydraulic capacity of the cylinder in node 5.

3. Analytical model

The system under consideration includes a long horizontal pipeline piece, an inclined pipeline piece, a short horizontal pipeline piece and a cylinder bore, which connect nodes 1–5 according to Figure 3. A state vector $\mathbf{p}$ is defined as

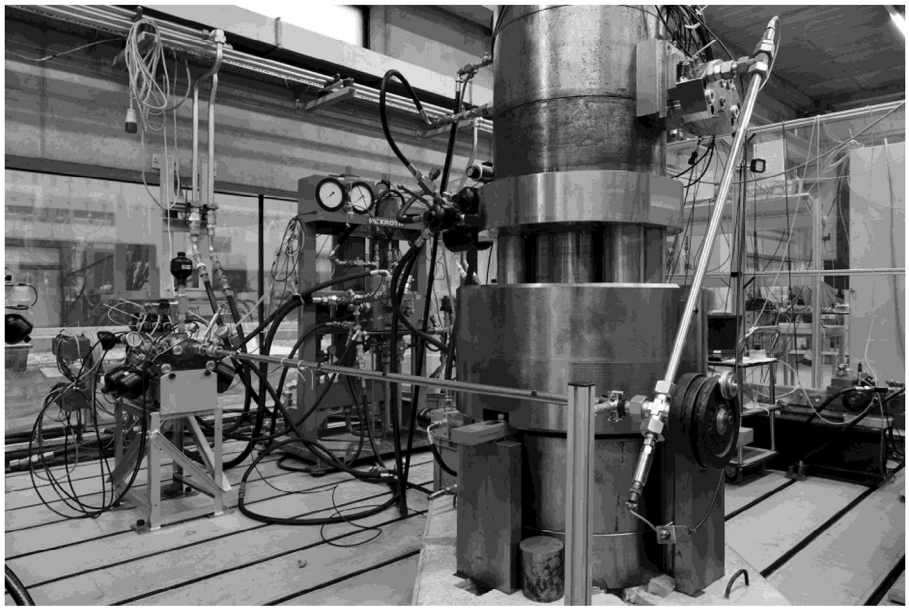

Figure 1. Experimental set-up.

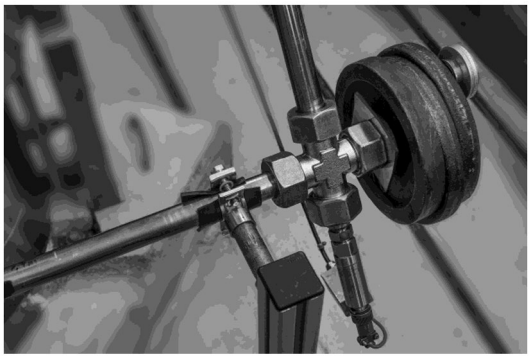

Figure 2. Attachment of additional mass.

$$\mathbf{p} = \left[\begin{array}{cccccccc} p_1 & v_{x1} & v_{y1} & \omega_1 & p_2 & v_{x2} & v_{y2} & \omega_2 \\ \cdots & p_4 & v_{x4} & v_{y4} & \omega_4 & p_5 & & \end{array} \right]^T \tag{1}$$

with pressures p_j in nodes j = 1–5 and velocities v_{xj}, v_{yj}, and angular velocities ω_j in nodes j = 1–4. The corresponding excitation vector

$$\mathbf{q} = \left[\begin{array}{cccccccc} q_1 & f_{x1} & f_{y1} & t_1 & q_2 & f_{x2} & f_{y2} & t_2 \\ \cdots & q_4 & f_{x4} & f_{y4} & t_4 & q_5 & & \end{array} \right]^T \tag{2}$$

contains flow rate excitations q_j in nodes j = 1–5 and excitation forces f_{xj},f_{yj}, and torques t_j in nodes j = 1–4. In the following, i denotes the imaginary unit and ω the angular frequency. It is intended to build up a frequency response matrix $\mathbf{G}$ which relates the Laplace transformed excitation vector $\mathbf{Q}$ and the Laplace transformed state vector $\mathbf{P}$ by

$$\mathbf{P}(\mathrm{i}\omega) = \mathbf{G}\mathbf{Q}(\mathrm{i}\omega); \tag{3}$$

since the frequency response functions $\mathbf{G}(1,1)$, $\mathbf{G}(5,1)$, $\mathbf{G}(6,1)$, $\mathbf{G}(7,1)$, and $\mathbf{G}(9,1)$ can be determined from measurements, this enables a validation of the model.

Considering frequency dependent friction, the hydraulic behaviour of a pipeline piece between nodes j and k is described by

$$\left[\begin{array}{cc} S_{jk} & T_{jk} \\ T_{jk} & S_{jk} \end{array} \right] \left[\begin{array}{c} P_j(\mathrm{i}\omega) \\ P_k(\mathrm{i}\omega) \end{array} \right] = \left[\begin{array}{c} Q_j(\mathrm{i}\omega) \\ Q_k(\mathrm{i}\omega) \end{array} \right] \tag{4}$$

with P_j, P_k, Q_j and Q_k as the Laplace transforms of p_j, p_k, q_j and q_k, respectively,

$$\left[\begin{array}{cc} S_{jk} & T_{jk} \\ T_{jk} & S_{jk} \end{array} \right] = \left[\begin{array}{cc} G_{jk} & H_{jk} \\ H_{jk} & G_{jk} \end{array} \right]^{-1}, \tag{5}$$

$$G_{jk} = \frac{\sqrt{E\rho} f(\mathrm{i}\omega)}{\mathrm{i}A} \cot\left(\frac{f(\mathrm{i}\omega)\omega l_{jk}}{\sqrt{E/\rho}} \right), \tag{6}$$

$$H_{jk} = \frac{\sqrt{E\rho} f(\mathrm{i}\omega)}{\mathrm{i}A} / \sin\left(\frac{f(\mathrm{i}\omega)\omega l_{jk}}{\sqrt{E/\rho}} \right), \tag{7}$$

and

$$f(\mathrm{i}\omega) = \sqrt{-\frac{J_0\left(\mathrm{i}r\sqrt{\mathrm{i}\omega/\nu}\right)}{J_2\left(\mathrm{i}r\sqrt{\mathrm{i}\omega/\nu}\right)}} \tag{8}$$

according to Mikota (2013). Symbols for system parameters are described in Table 1, and J_0 and J_2 denote Bessel functions of first kind.

On the mechanical side, undamped axial tension behaves like the frictionless case of Equations (4–8); in the appropriate state variables, this reads

$$\left[\begin{array}{cc} Q_{jk} & R_{jk} \\ R_{jk} & Q_{jk} \end{array} \right] \left[\begin{array}{c} V_{aj}(\mathrm{i}\omega) \\ V_{ak}(\mathrm{i}\omega) \end{array} \right] = \left[\begin{array}{c} F_{aj}(\mathrm{i}\omega) \\ F_{ak}(\mathrm{i}\omega) \end{array} \right] \tag{9}$$

with V_{aj}, V_{ak}, F_{aj} and F_{ak} as Laplace transformed axial velocities and forces, respectively,

$$Q_{jk} = \frac{\sqrt{E_w\rho_w} A_w}{\mathrm{i}} \cot\left(\frac{\omega l_{jk}}{\sqrt{E_w/\rho_w}} \right), \tag{10}$$

and

$$R_{jk} = -\frac{\sqrt{E_w\rho_w} A_w}{\mathrm{i}} / \sin\left(\frac{\omega l_{jk}}{\sqrt{E_w/\rho_w}} \right). \tag{11}$$

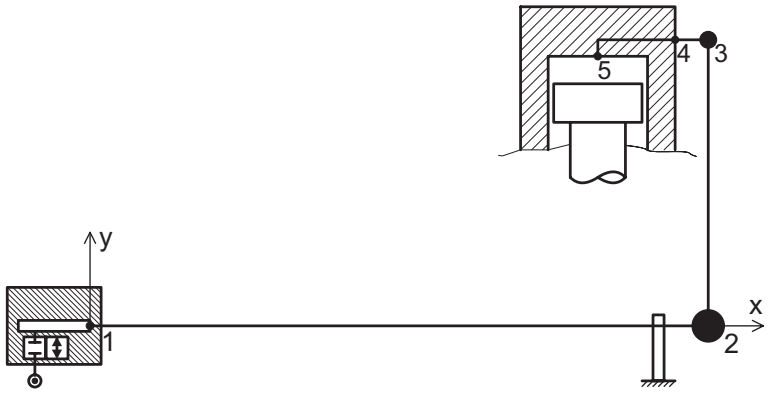

Figure 3. Simplified schematic of experimental set-up.

Table 1. System parameters.

	Symbol	Value
Fluid bulk modulus	E	$1.5 \cdot 10^9$ Pa
Fluid density	ρ	860 kg m^{-3}
Kinematic viscosity of fluid	ν	$5 \cdot 10^{-5}$ m^{2}s^{-1}
Internal pipeline radius	r	$9.45 \cdot 10^{-3}$ m
Internal pipeline cross-sectional area	A	$2.81 \cdot 10^{-4}$ m^2
Pipeline wall elastic modulus	E_w	$2.1 \cdot 10^{11}(1 + 0.02\mathrm{i})$ Pa
Pipeline wall density	ρ_w	7800 kg m^{-3}
Pipeline wall cross-sectional area	A_w	$2.06 \cdot 10^{-4}$ m^2
Pipeline wall area moment of inertia	J_w	$1.26 \cdot 10^{-8}$ m^4
Length of long horizontal pipeline piece	l_{12}	2.235 m
Length of inclined pipeline piece	l_{23}	1.040 m
Length of short horizontal pipeline piece	l_{34}	0.117 m
Length of cylinder bore	l_{45}	0.370 m
Fluid volume inside valve block	V_1	$0.3 \cdot 10^{-3}$ m^3
Fluid volume inside cylinder	V_5	0.1 m^3
Valve block mass	m_1	100 kg
Valve block mass moment of inertia	I_1	2 kg m^2
Position of valve block centre of gravity	x_1	−0.14 m
Fitting and sensor mass at first pipeline bend	m_2	1.7 kg
Compensator mass	m_{2c}	8.154 kg
Fitting and sensor mass at second pipeline bend	m_3	1.35 kg
Cylinder mass	m_4	800 kg
Cylinder mass moment of inertia	I_4	60 kg m^2

Structural damping can be taken into account by an imaginary part of the pipeline wall elastic modulus E_w.

Pipeline bending is described by the ordinary differential equation

$$E_w J_w \frac{\partial^4 W(\xi, s)}{\partial \xi^4} + \rho_w A_w s^2 W(\xi, s) = 0 \tag{12}$$

for the Laplace transformed lateral deflection $W(\xi, s)$, where ξ is the coordinate along the pipeline axis, and s denotes the Laplace variable. According to Thomson and Dahleh (1998), the general solution of Equation (12) reads

$$\begin{aligned} W(\xi, s) = {} & A \cosh(\beta\xi) + B \sinh(\beta\xi) \\ & + C \cos(\beta\xi) + D \sin(\beta\xi), \end{aligned} \tag{13}$$

and

$$\beta^4 = -\frac{\rho_w A_w}{E_w J_w} s^2. \tag{14}$$

Deflection and slope at both pipeline ends are given as

$$W(0, s) = A + C \tag{15}$$

$$W'(0, s) = \beta(B + D) \tag{16}$$

$$\begin{aligned} W\left(l_{jk}, s\right) = {} & A \cosh\left(\beta l_{jk}\right) + B \sinh\left(\beta l_{jk}\right) \\ & + C \cos\left(\beta l_{jk}\right) + D \sin\left(\beta l_{jk}\right) \end{aligned} \tag{17}$$

$$\begin{aligned} W'\left(l_{jk}, s\right) = \beta\Big(& A \sinh\left(\beta l_{jk}\right) + B \cosh\left(\beta l_{jk}\right) \\ & - C \sin\left(\beta l_{jk}\right) + D \cos\left(\beta l_{jk}\right)\Big) \end{aligned} \tag{18}$$

such that

$$\begin{bmatrix} A \\ B \\ C \\ D \end{bmatrix} = \mathbf{E}(s) \begin{bmatrix} W(0, s) \\ W'(0, s) \\ W\left(l_{jk}, s\right) \\ W'\left(l_{jk}, s\right) \end{bmatrix} \tag{19}$$

with

$$\mathbf{E}(s) = \begin{bmatrix} 1 & 0 & 1 & 0 \\ 0 & \beta & 0 & \beta \\ \cosh\left(\beta l_{jk}\right) & \sinh\left(\beta l_{jk}\right) & \cos\left(\beta l_{jk}\right) & \sin\left(\beta l_{jk}\right) \\ \beta \sinh\left(\beta l_{jk}\right) & \beta \cosh\left(\beta l_{jk}\right) & -\beta \sin\left(\beta l_{jk}\right) & \beta \cos\left(\beta l_{jk}\right) \end{bmatrix}^{-1}. \tag{20}$$

Using the expressions

$$M(\xi, s) = -E_w J_w W''(\xi, s) \tag{21}$$

for Laplace transformed bending moment and

$$F_l(\xi, s) = -E_w J_w W'''(\xi, s) \tag{22}$$

for Laplace transformed lateral force, the relations

$$F_l(0, s) = -E_w J_w \beta^3 (B - D) \tag{23}$$

$$M(0, s) = -E_w J_w \beta^2 (A - C) \tag{24}$$

$$\begin{aligned} F_l\left(l_{jk}, s\right) = -E_w J_w \beta^3 \Big(& A \sinh\left(\beta l_{jk}\right) + B \cosh\left(\beta l_{jk}\right) \\ & + C \sin\left(\beta l_{jk}\right) - D \cos\left(\beta l_{jk}\right)\Big) \end{aligned} \tag{25}$$

$$\begin{aligned} M\left(l_{jk}, s\right) = -E_w J_w \beta^2 \Big(& A \cosh\left(\beta l_{jk}\right) + B \sinh\left(\beta l_{jk}\right) \\ & - C \cos\left(\beta l_{jk}\right) - D \sin\left(\beta l_{jk}\right)\Big) \end{aligned} \tag{26}$$

are obtained at the pipeline ends and can be summarised as

$$\mathbf{F}(s) \begin{bmatrix} A \\ B \\ C \\ D \end{bmatrix} = \begin{bmatrix} F_l(0, s) \\ M(0, s) \\ F_l\left(l_{jk}, s\right) \\ M\left(l_{jk}, s\right) \end{bmatrix} \tag{27}$$

with

$$\mathbf{F}(s) = -E_w J_w \beta^2 \begin{bmatrix} 0 & \beta & 0 & -\beta \\ 1 & 0 & -1 & 0 \\ \beta \sinh\left(\beta l_{jk}\right) & \beta \cosh\left(\beta l_{jk}\right) & \beta \sin\left(\beta l_{jk}\right) & -\beta \cos\left(\beta l_{jk}\right) \\ \cosh\left(\beta l_{jk}\right) & \sinh\left(\beta l_{jk}\right) & -\cos\left(\beta l_{jk}\right) & -\sin\left(\beta l_{jk}\right) \end{bmatrix}. \tag{28}$$

Combining Equations (19) and (27), taking the time derivative of lateral deflection in the Laplace domain, and setting $s = \mathrm{i}\omega$ leads to the matrix description

$$\mathbf{U}_{jk}(\mathrm{i}\omega)\begin{bmatrix} V_{lj}(\mathrm{i}\omega) \\ V'_{lj}(\mathrm{i}\omega) \\ V_{lk}(\mathrm{i}\omega) \\ V'_{lk}(\mathrm{i}\omega) \end{bmatrix} = \begin{bmatrix} F_{lj}(\mathrm{i}\omega) \\ M_{j}(\mathrm{i}\omega) \\ F_{lk}(\mathrm{i}\omega) \\ M_{k}(\mathrm{i}\omega) \end{bmatrix} \tag{29}$$

of pipeline bending, in which V_{lj}, V_{lk}, V'_{lj} and V'_{lk} are Laplace transformed lateral velocities and angular velocities, respectively,

$$\mathbf{U}_{jk}(\mathrm{i}\omega) = \frac{1}{\mathrm{i}\omega}\mathbf{F}(\mathrm{i}\omega)\mathbf{E}(\mathrm{i}\omega), \tag{30}$$

and

$$\beta = \sqrt{\sqrt{\frac{\rho_w A_w}{E_w J_w}}\omega}. \tag{31}$$

For later use, the elements of the matrix $\mathbf{U}_{jk}(\mathrm{i}\omega)$ are denoted by

$$\mathbf{U}_{jk} = \begin{bmatrix} U_{jk}^{a)} & U_{jk}^{b)} & U_{jk}^{c)} & U_{jk}^{d)} \\ U_{jk}^{e)} & U_{jk}^{f)} & U_{jk}^{g)} & U_{jk}^{h)} \\ U_{jk}^{i)} & U_{jk}^{j)} & U_{jk}^{k)} & U_{jk}^{l)} \\ U_{jk}^{m)} & U_{jk}^{n)} & U_{jk}^{o)} & U_{jk}^{p)} \end{bmatrix}. \tag{32}$$

It is noted that the directions of lateral velocities, angular velocities, lateral forces and bending moments follow usual beam theory conventions (Thomson and Dahleh 1998); if both velocities and forces as well as moments comply with coordinate directions in Figure 3, the signs of the matrix elements in Equation (32) must be adapted for each pipeline piece.

Local inverse frequency response matrices of the individual pipeline pieces are based on Equations (4), (9), and (29). Appropriate dynamic descriptions of discrete hydraulic capacities and mechanical masses are added in accordance with continuity and force balance in the system nodes. Coupling forces occur from hydraulic pressure at the pipeline piece ends, where axial velocities lead to corresponding coupling flow rates. In the coordinate system from Figure 3, the local inverse frequency response matrix of the long horizontal pipeline piece thus becomes

$$\mathbf{S}_{lhpp} = \begin{bmatrix} S_{12}+\mathrm{i}\omega C_1 & -A & 0 & 0 & T_{12} & 0 & 0 & 0 \\ A & Q_{12}+\mathrm{i}\omega m_1 & 0 & 0 & 0 & R_{12} & 0 & 0 \\ 0 & 0 & -U_{12}^{a)}+\mathrm{i}\omega m_1 & -U_{12}^{b)}+\mathrm{i}\omega x_1 m_1 & 0 & 0 & -U_{12}^{c)} & -U_{12}^{d)} \\ 0 & 0 & U_{12}^{e)} & U_{12}^{f)}+\mathrm{i}\omega I_1 & 0 & 0 & U_{12}^{g)} & U_{12}^{h)} \\ T_{12} & 0 & 0 & 0 & S_{12} & A & 0 & 0 \\ 0 & R_{12} & 0 & 0 & -A & Q_{12}+\mathrm{i}\omega m_2 & 0 & 0 \\ 0 & 0 & U_{12}^{i)} & U_{12}^{j)} & 0 & 0 & U_{12}^{k)}+\mathrm{i}\omega m_2 & U_{12}^{l)} \\ 0 & 0 & -U_{12}^{m)} & -U_{12}^{n)} & 0 & 0 & -U_{12}^{o)} & -U_{12}^{p)} \end{bmatrix} \tag{33}$$

with a valve block capacity $C_1 = V_1/E$ and system parameters according to Table 1. However, the fluid viscosity ν is increased to account for the flow resistance of fittings along the pipeline. An intermediate fitting also changes the mechanical behaviour of the long horizontal pipeline piece, which is taken into account by adapting the pipeline wall elastic modulus E_{w12}. These adjustments are based on a comparison between measured and calculated frequency response functions and will be detailed in Section 4. The local inverse frequency response matrix of the inclined pipeline piece is given as

$$\mathbf{S}_{ipp} = \begin{bmatrix} S_{23} & 0 & -A & 0 & T_{23} & 0 & 0 & 0 \\ 0 & -U_{23}^{a)} & 0 & U_{23}^{b)} & 0 & -U_{23}^{c)} & 0 & U_{23}^{d)} \\ A & 0 & Q_{23} & 0 & 0 & 0 & R_{23} & 0 \\ 0 & -U_{23}^{e)} & 0 & U_{23}^{f)} & 0 & -U_{23}^{g)} & 0 & U_{23}^{h)} \\ T_{23} & 0 & 0 & 0 & S_{23} & 0 & A & 0 \\ 0 & U_{23}^{i)} & 0 & -U_{23}^{j)} & 0 & U_{23}^{k)}+\mathrm{i}\omega m_3 & 0 & -U_{23}^{l)} \\ 0 & 0 & R_{23} & 0 & -A & 0 & Q_{23}+\mathrm{i}\omega m_3 & 0 \\ 0 & U_{23}^{m)} & 0 & -U_{23}^{n)} & 0 & U_{23}^{o)} & 0 & -U_{23}^{p)} \end{bmatrix}, \tag{34}$$

and the local inverse frequency response matrix of the short horizontal pipeline piece reads

$$\mathbf{S}_{shpp} = \begin{bmatrix} S_{34} & A & 0 & 0 & T_{34} & 0 & 0 & 0 \\ -A & Q_{34} & 0 & 0 & 0 & R_{34} & 0 & 0 \\ 0 & 0 & -U_{34}^{a)} & U_{34}^{b)} & 0 & 0 & -U_{34}^{c)} & U_{34}^{d)} \\ 0 & 0 & -U_{34}^{e)} & U_{34}^{f)} & 0 & 0 & -U_{34}^{g)} & U_{34}^{h)} \\ T_{34} & 0 & 0 & 0 & S_{34} & -A & 0 & 0 \\ 0 & R_{34} & 0 & 0 & A & Q_{34}+\mathrm{i}\omega m_4 & 0 & 0 \\ 0 & 0 & U_{34}^{i)} & -U_{34}^{j)} & 0 & 0 & U_{34}^{k)}+\mathrm{i}\omega m_4 & -U_{34}^{l)} \\ 0 & 0 & U_{34}^{m)} & -U_{34}^{n)} & 0 & 0 & U_{34}^{o)} & -U_{34}^{p)}+\mathrm{i}\omega I_4 \end{bmatrix}. \tag{35}$$

Since the short horizontal pipeline piece mainly consists of fittings, the area moment of inertia J_{w34} will be adjusted by a comparison between measured and calculated frequency response functions to obtain a realistic bending stiffness. The inertia of the cylinder is very large and will almost lock the mechanical degrees of freedom in node 4; therefore, Table 1 only gives rough estimates of the parameters m_4 and I_4, and the distance between node 4 an the cylinder centre of gravity is not taken into account.

For the cylinder bore, rigid walls are assumed, and equations reduce to the purely hydraulic case. The local inverse frequency response matrix then reads

$$\mathbf{S}_{cb} = \begin{bmatrix} S_{45} & 0 & 0 & 0 & T_{45} \\ 0 & 0 & 0 & 0 & 0 \\ 0 & 0 & 0 & 0 & 0 \\ 0 & 0 & 0 & 0 & 0 \\ T_{45} & 0 & 0 & 0 & S_{45}+\mathrm{i}\omega C_5 \end{bmatrix}; \tag{36}$$

the influence of the cylinder is approximated by a large capacity $C_5 = V_5/E$. With global inverse frequency response matrices expanded to the full system dimension, continuity and force balance enable the superposition

$$\begin{bmatrix} \mathbf{S}_{lhpp} & \mathbf{0}_{8\times9} \\ \mathbf{0}_{9\times8} & \mathbf{0}_{9\times9} \end{bmatrix} + \begin{bmatrix} \mathbf{0}_{4\times4} & \mathbf{0}_{4\times8} & \mathbf{0}_{4\times5} \\ \mathbf{0}_{8\times4} & \mathbf{S}_{ipp} & \mathbf{0}_{8\times5} \\ \mathbf{0}_{5\times4} & \mathbf{0}_{5\times8} & \mathbf{0}_{5\times5} \end{bmatrix} + \begin{bmatrix} \mathbf{0}_{8\times8} & \mathbf{0}_{8\times8} & \mathbf{0}_{8\times1} \\ \mathbf{0}_{8\times8} & \mathbf{S}_{shpp} & \mathbf{0}_{8\times1} \\ \mathbf{0}_{1\times8} & \mathbf{0}_{1\times8} & \mathbf{0}_{1\times1} \end{bmatrix} + \begin{bmatrix} \mathbf{0}_{12\times12} & \mathbf{0}_{12\times5} \\ \mathbf{0}_{5\times12} & \mathbf{S}_{cb} \end{bmatrix} = \mathbf{G}^{-1}, \tag{37}$$

from which the frequency response matrix $\mathbf{G}$ according to Equation (3) can be determined.

4. Experiment without additional mass

In a first experiment, the dynamic behaviour of the original pipeline is investigated; the additional mass is not attached. The pipeline is excited by a 2 ms flow rate pulse from supply. Valve spool position, pressure and acceleration signals are collected via dSPACE. Using the orifice equation, the flow rate excitation q_1 is reconstructed from the measured valve spool position and the measured pressure p_1 assuming a constant supply pressure of 20 MPa. Frequency response functions between the flow rate q_1

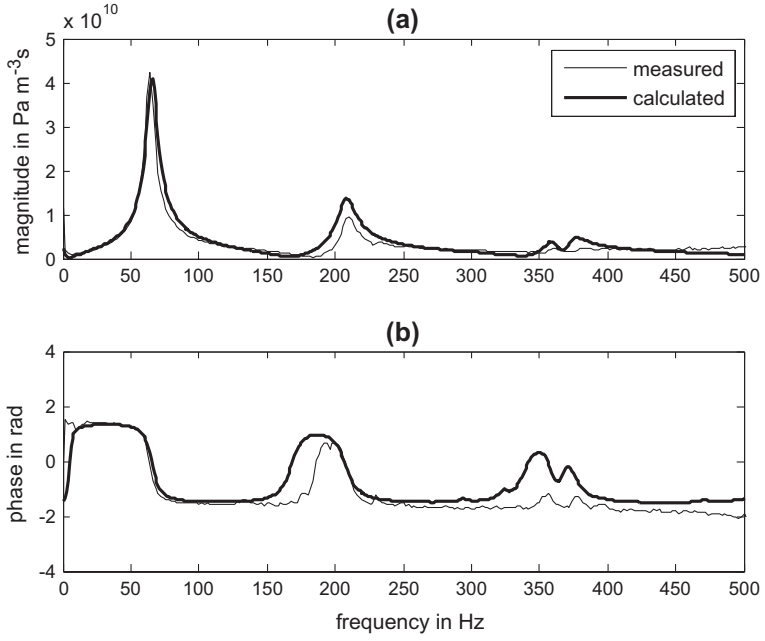

Figure 4. Without additional mass: frequency response functions between flow rate q_1 and pressure p_1. (a) magnitude, (b) phase.

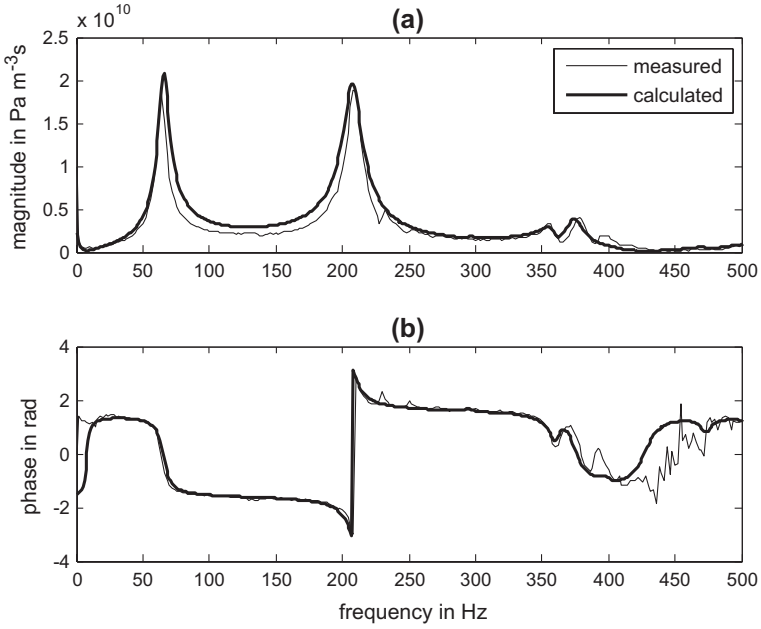

Figure 5. Without additional mass: frequency response functions between flow rate q_1 and pressure p_2. (a) magnitude, (b) phase.

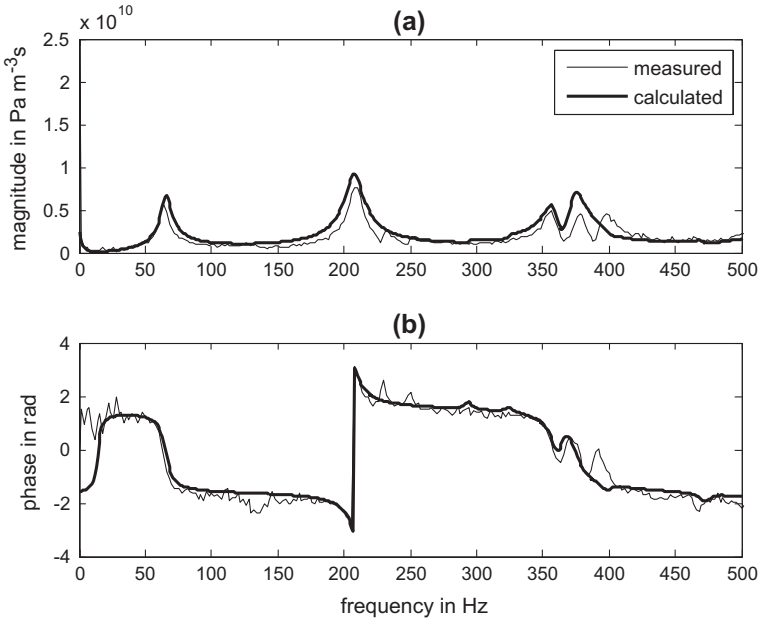

Figure 6. Without additional mass: frequency response functions between flow rate q_1 and pressure p_3. (a) magnitude, (b) phase.

and the pressures p_1, p_2 and p_3 as well as the velocities v_{x2}, v_{y2} and v_{z2} are determined by Matlab. These measured frequency response functions are shown in Figures 4–9 along with their calculated counterparts from the model in Section 3. Figure 9 only shows a measured result since the plane model does not consider a velocity v_{z2}.

To match the first and second hydraulic resonances, the calculation uses an increased kinematic viscosity of $\nu = 2.3 \cdot 10^{-4}\ \mathrm{m^2 s^{-1}}$. The triple peak around the third hydraulic resonance only appears with appropriate changes in structural parameters. The calculated frequency response functions in Figures 4–8 are obtained for a pipeline wall elastic modulus $E_{w12} = 0.78 \cdot E_w$ between nodes 1 and 2 and an area moment of inertia $J_{w34} = 7 \cdot J_w$ between nodes 3 and 4. Figures 4–6 show fair agreement between measured and calculated pressure responses although the triple peak is somewhat distorted by the model. In Figures 7 and 8, measured and calculated velocity responses are the same order of magnitude, but differences appear in the frequency content. This may be explained by the influence of the pillar, which also causes some out-of-plane vibrations as shown in Figure 9. However, out-of-plane magnitudes are considerably smaller than those in directions x and y.

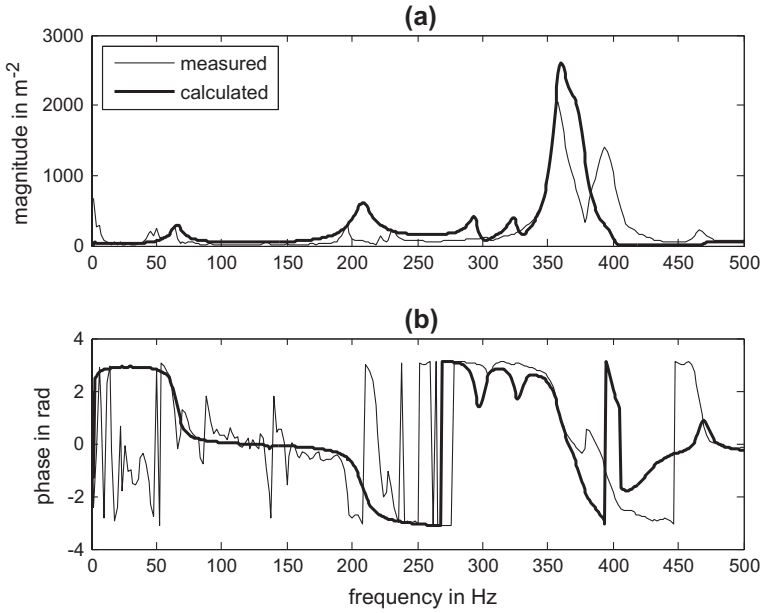

Figure 7. Without additional mass: frequency response functions between flow rate q_1 and velocity v_{x2}. (a) magnitude, (b) phase.

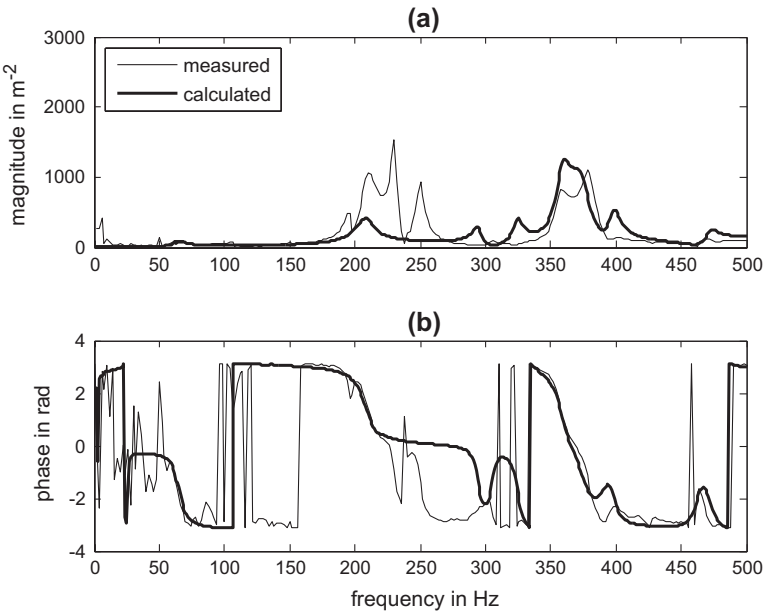

Figure 8. Without additional mass: frequency response functions between flow rate q_1 and velocity v_{y2}. (a) magnitude, (b) phase.

5. Experiment with additional mass

In Figures 4–6, the triple peak around the third hydraulic resonance is an obvious result of fluid–structure interaction. Two natural frequencies of the pipeline structure come near the third hydraulic natural frequency of the pipeline. The coincidence of natural frequencies is a well-known condition for vibration compensation; to some extent, the pipeline structure acts as a compensator for the third hydraulic resonance. It will be possible to compensate the second hydraulic resonance if the structure is tuned in a suitable way. The natural frequencies of the pipeline structure can efficiently be lowered by adding a mass in the most flexible part of the pipeline. Therefore, an additional mass is attached at the first pipeline bend. The appropriate size of the mass is determined by several experiments in which the vibration response to hammer excitation at the first pipeline bend is evaluated by an FFT analyser; this procedure shows the natural frequencies of the pipeline structure and indicates the required changes in mass. The final compensator mass m_{2c} is given in Table 1.

Frequency response functions from hydraulic excitation of the pipeline with the additional compensator mass are shown in Figures 10–15. To match measured and calculated magnitudes around the second

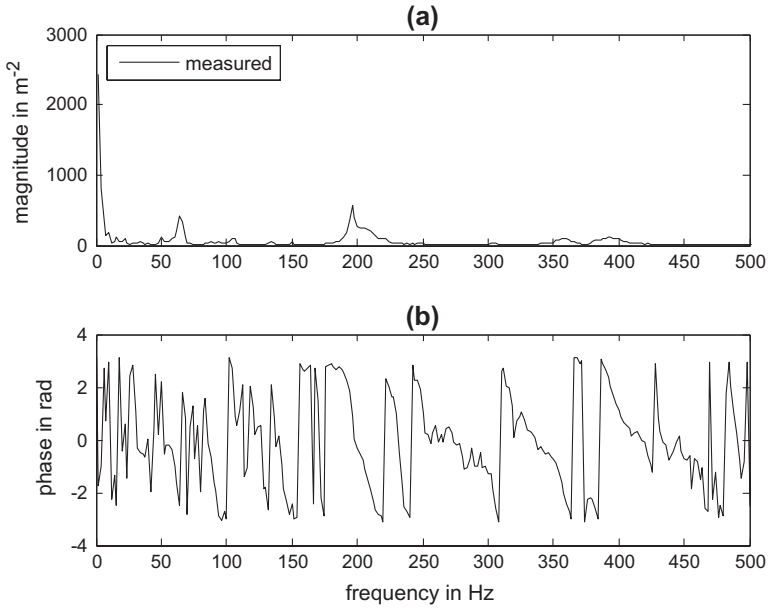

Figure 9. Without additional mass: frequency response function between flow rate q_1 and velocity v_{z2}. (a) magnitude, (b) phase.

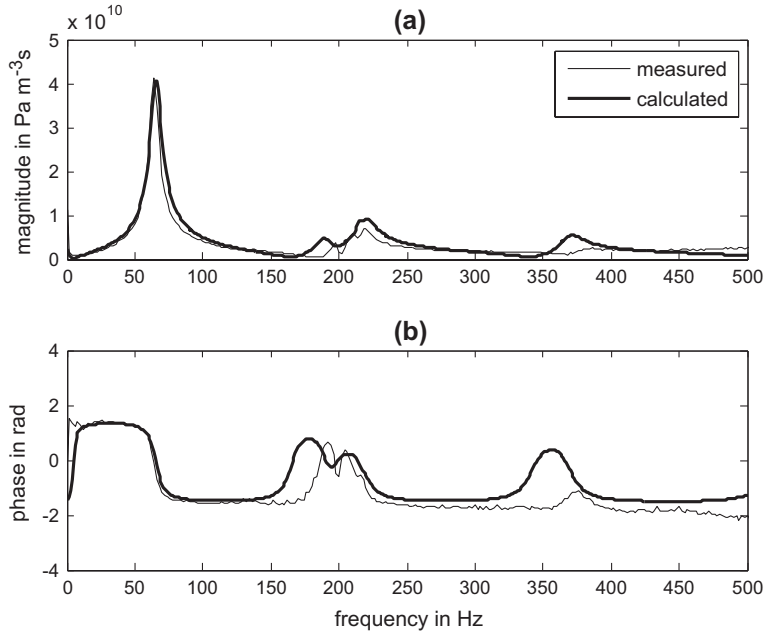

Figure 10. With additional mass: frequency response functions between flow rate q_1 and pressure p_1. (a) magnitude, (b) phase.

hydraulic resonance, the attachment of the compensator mass must not be considered as rigid. This attachment is efficiently modelled by viscous dampers in x- and y-direction, whose damping constants are set to $c_{xa} = c_{ya} = 1.5 \cdot 10^5$ Nsm^{-1}. Consequently, the state vector $\mathbf{p}$ is extended to include the velocities v_{xc} and v_{yc} of the compensator mass so that the extended state vector reads

$$\mathbf{p}_e = \begin{bmatrix} \mathbf{p}^T & v_{xc} & v_{yc} \end{bmatrix}^T; \tag{38}$$

its Laplace transform $\mathbf{P}_e$ is related to the Laplace transform $\mathbf{Q}_e$ of the extended excitation vector

$$\mathbf{q}_e = \begin{bmatrix} \mathbf{q}^T & f_{xc} & f_{yc} \end{bmatrix}^T \tag{39}$$

by

$$\mathbf{P}_e(\mathrm{i}\omega) = \mathbf{G}_e\mathbf{Q}_e(\mathrm{i}\omega), \tag{40}$$

in which the extended frequency response matrix $\mathbf{G}_e$ can be determined from

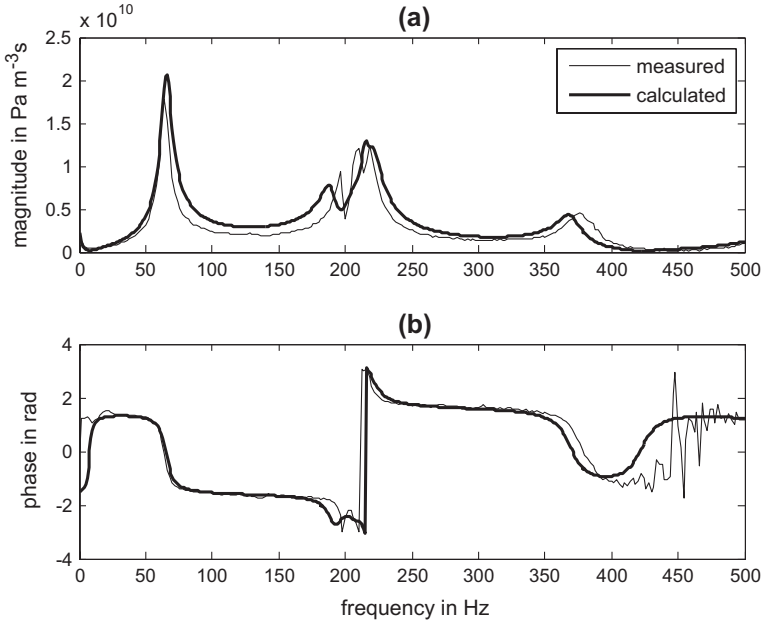

Figure 11. With additional mass: frequency response functions between flow rate q_1 and pressure p_2. (a) magnitude, (b) phase.

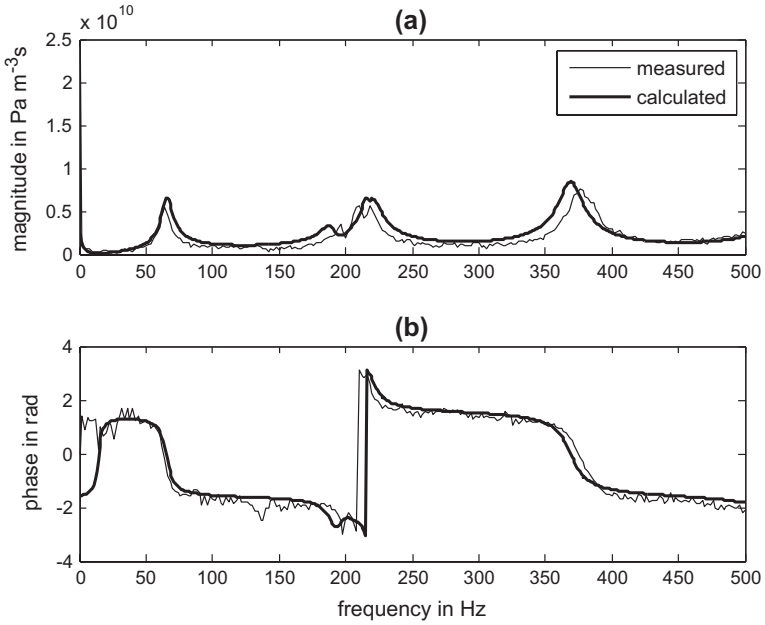

Figure 12. With additional mass: frequency response functions between flow rate q_1 and pressure p_3. (a) magnitude, (b) phase.

$$\mathbf{G}_e^{-1} = \begin{bmatrix} \mathbf{G}^{-1} & \mathbf{0}_{17\times2} \\ \mathbf{0}_{2\times17} & \mathbf{0}_{2\times2} \end{bmatrix} + \begin{bmatrix} \mathbf{0}_{5\times5} & \mathbf{0}_{5\times1} & \mathbf{0}_{5\times1} & \mathbf{0}_{5\times10} & \mathbf{0}_{5\times1} & \mathbf{0}_{5\times1} \\ \mathbf{0}_{1\times5} & c_{xa} & 0 & \mathbf{0}_{1\times10} & -c_{xa} & 0 \\ \mathbf{0}_{1\times5} & 0 & c_{ya} & \mathbf{0}_{1\times10} & 0 & -c_{ya} \\ \mathbf{0}_{10\times5} & \mathbf{0}_{10\times1} & \mathbf{0}_{10\times1} & \mathbf{0}_{10\times10} & \mathbf{0}_{10\times1} & \mathbf{0}_{10\times1} \\ \mathbf{0}_{1\times5} & -c_{xa} & 0 & \mathbf{0}_{1\times10} & c_{xa}+\mathrm{i}\omega m_{2c} & 0 \\ \mathbf{0}_{1\times5} & 0 & -c_{ya} & \mathbf{0}_{1\times10} & 0 & c_{ya}+\mathrm{i}\omega m_{2c} \end{bmatrix} \tag{41}$$

with the frequency response matrix $\mathbf{G}$ according to Equation (37). Figures 10–12 show that this extension of the model leads to good agreement between measured and calculated pressure responses. By adding the compensator mass, the triple peak has in fact been shifted from the third hydraulic resonance to the second. A comparison of Figures 5 and 11 demonstrates that near the second hydraulic resonance, the maximum pressure

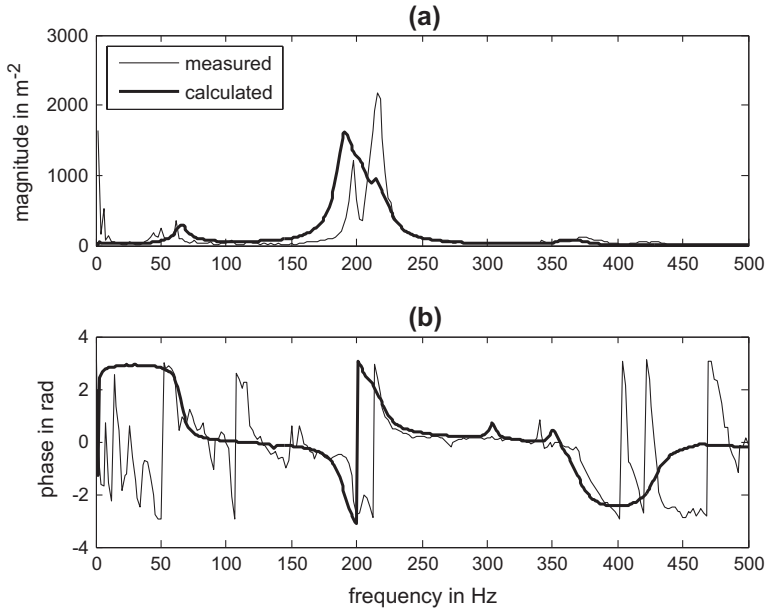

Figure 13. With additional mass: frequency response functions between flow rate q_1 and velocity v_{x2}. (a) magnitude, (b) phase.

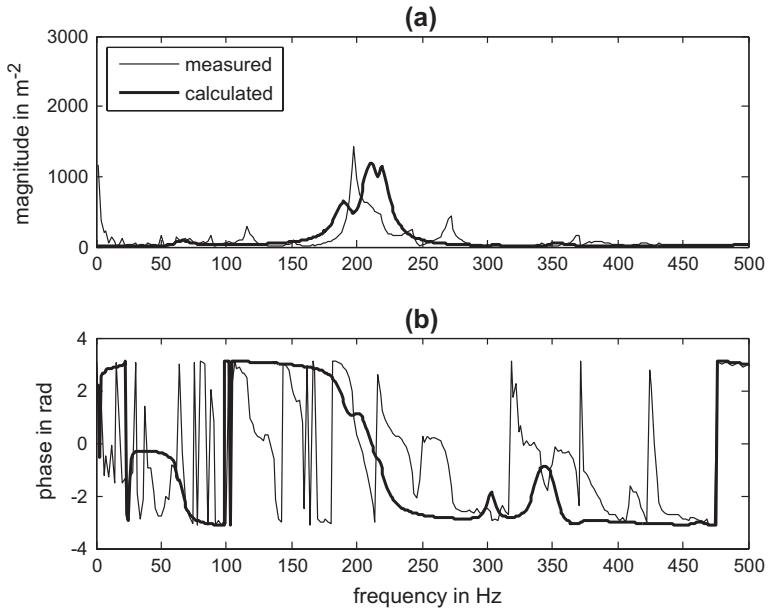

Figure 14. With additional mass: frequency response functions between flow rate q_1 and velocity v_{y2}. (a) magnitude, (b) phase.

magnitude at the first pipeline bend has been reduced to 65%. Measured and calculated velocity responses roughly agree in Figures 13 and 14; the remaining differences may be explained by the influence of the pillar, which also causes out-of-plane vibrations as shown in Figure 15. Out-of-plane magnitudes are still smaller than in-plane ones; for an approximation, this justifies the use of a plane model that neglects the pillar.

6. Experiments with additional mass and damper

Vibration compensators can be optimised by an adjustment of damping. In the present experiments, this is attempted by inserting a layer of rubber between the pipeline and the compensator mass. Experiments are made with a 5-mm and a 3-mm layer of rubber. For all tested configurations, Figure 16 shows the relevant detail of measured frequency response functions between flow rate excitation and pressure response at the first pipeline bend. Although a direct attachment of the mass gives the largest reduction in magnitude, intermediate results are obtained with different layers of rubber. The damped configuration can still be described by the extended model from Section 5. The 5-mm rubber is modelled by attachment damping constants $c_{xa} = 8000\ \mathrm{Nsm^{-1}}$ and $c_{ya} = 0\ \mathrm{Nsm^{-1}}$; for the 3-mm rubber, $c_{xa} = 14000\ \mathrm{Nsm^{-1}}$ and $c_{ya} = 0\ \mathrm{Nsm^{-1}}$. Figure 17 shows the calculated

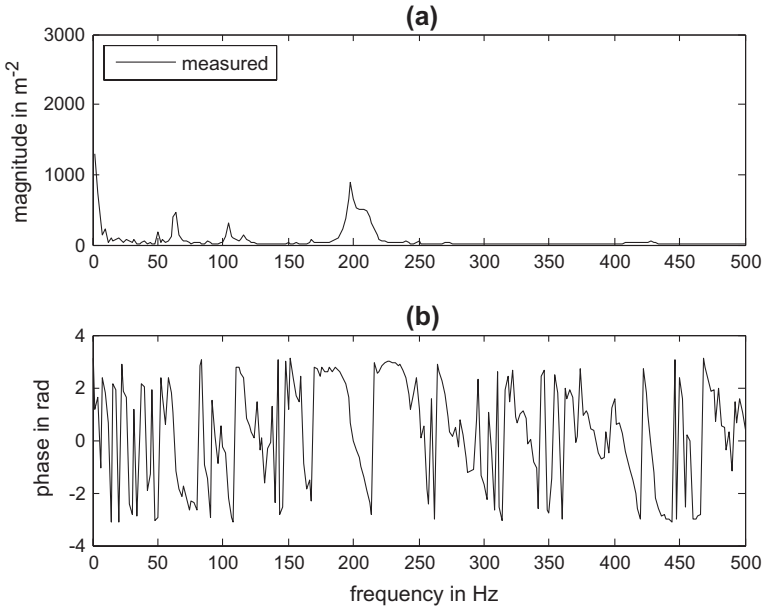

Figure 15. With additional mass: frequency response function between flow rate q_1 and velocity v_{z2}. (a) magnitude, (b) phase.

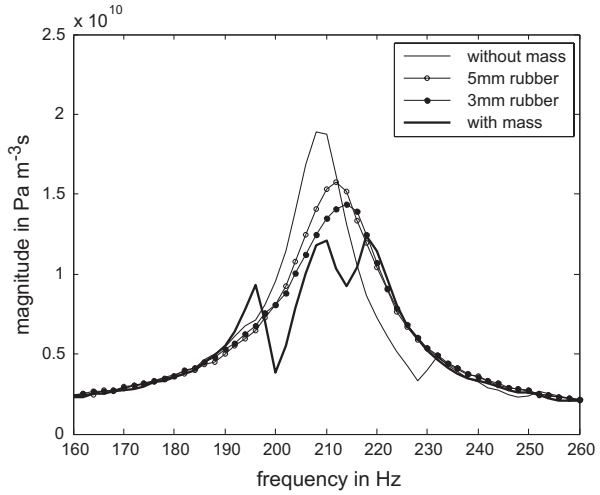

Figure 16. Measured frequency response functions between flow rate q_1 and pressure p_2; detail of magnitude around second hydraulic resonance.

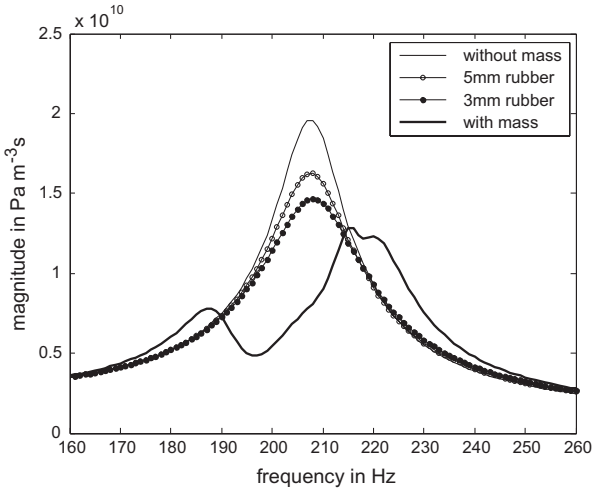

Figure 17. Calculated frequency response functions between flow rate q_1 and pressure p_2; detail of magnitude around second hydraulic resonance.

counterparts of the measured magnitudes in Figure 16. The model generates two intermediate results, which resemble the respective measurements.

7. Conclusions

Fluid–structure interaction has been studied for a hydraulic pipeline between a valve block and a cylinder. By adding a mass of 8.154 kg at the first pipeline bend, the second hydraulic pipeline resonance peak has been successfully compensated. In the respective frequency range, the maximum magnitude of the pressure at the first pipeline bend has been reduced to 65%. This may be useful for the dynamic performance of the overall drive and demonstrates that the hydraulic behaviour of a pipeline can be changed by appropriate measures in the pipeline structure.

A plane frequency domain model has been validated against measurements on the pipeline with and without additional mass and with different layers of rubber in between. Calculated frequency response functions between flow rate excitation and pressure response are in good agreement with their measured counterparts; the model also provides a rough approximation of structural vibrations. This would be improved by considering a third spatial dimension and including the pillar that supports the pipeline. Further improvements could be expected from a separate update of the

structural model, an inclusion of cylinder dynamics and an extension of the fluid–structure interaction model beyond junction coupling. However, the simplified model in this paper clearly reproduces the measured compensation effect.

Disclosure statement

No potential conflict of interest was reported by the authors.

Funding

This work has been carried out at LCM GmbH as part of a K2 project. K2 projects are financed using funding from the Austrian COMET-K2 programme. The COMET K2 projects at LCM are supported by the Austrian federal government, the federal state of Upper Austria, the Johannes Kepler University and all of the scientific partners which form part of the K2-COMET Consortium.

Notes on contributors

Gudrun Mikota studied mechanical engineering at Vienna University of Technology, where she received her PhD in 2001. She worked with Jenbacher AG and LCM GmbH in the fields of vibration engineering and fluid power systems. Currently, she is a senior scientist at the JKU Institute of Machine Design and Hydraulic Drives.

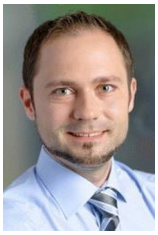

Rainer Haas studied mechatronics at the JKU Linz and was a research assistant at the Institute of Machine Design and Hydraulic Drives, where he received his PhD in 2013. His thesis deals with identification of fluid compressibility and simulation of wave propagation including non-linear fluid laws. He is currently employed as a senior engineer at the LCM GmbH.

Evgeny Lukachev graduated in 2007 from Bauman Moscow State Technical University in Kaluga, Russia. He worked as an engineer in the power plant turbine industry and in the development of electric drives before beginning as a PhD student at the JKU Linz in 2012. The topic of his research is hydraulic drives with fast switching valve control.

References

Ingard, U., 1953. On the theory and design of acoustic resonators. *Journal of the acoustical society of America*, 25 (6), 1037–1061.

Lavooij, C.S.W. and Tijsseling, A.S., 1991. Fluid-structure interaction in liquid-filled piping systems. *Journal of fluids and structures*, 5, 573–595.

Li, X., Wang, S., and Liang, R., 2011. Modal analysis of two typical fluid-filled pipes in aircraft. *In*: *International conference on fluid power and mechatronics*. Beijing: IEEE, 462–466.

Liu, G. and Li, Y., 2011. Vibration analysis of liquid-filled pipelines with elastic constraints. *Journal of sound and vibration*, 330, 3166–3181.

Liu, G., *et al.*, 2013. Vibration analysis of pipelines with arbitrary branches by absorbing transfer matrix method. *Journal of sound and vibration*, 332, 6519–6536.

Makaryants, G.M., Prokofiev, A.B. and Shakhmatov, E.V., 2015. Vibroacoustics analysis of punching machine hydraulic piping. *Procedia engineering*, 106, 17–26.

Mikota, G., 2013. Modal analysis of hydraulic pipelines. *Journal of sound and vibration*, 332, 3794–3805.

Mikota, G., *et al.*, 2016a. Experimentelle Modalanalyse eines gekoppelten hydraulisch-mechanischen Systems. *In*: *4. VDI-Fachtagung Schwingungsanalyse & Identifikation 2016*, 15–16 March 2016 Fulda. VDI-Berichte 2259, Düsseldorf: VDI Verlag GmbH, 97–108.

Mikota, G., Haas, R., and Lukachev, E., 2016b. Modal analysis of fluid-structure interaction in a bent pipeline. *In*: *2016 Bath/ASME symposium on fluid power and motion control*, 7–9 September 2016 Bath. ASME, FPMC2016-1705.

Mikota, J., 2002. *Contributions to the development of compact and tuneable vibration compensators for hydraulic systems*. Thesis (PhD). Johannes Kepler University Linz.

Mikota, J. and Reiter, H., 2003. Development of a compact and tuneable vibration compensator for hydraulic systems. *International journal of fluid power*, 4 (1), 17–31.

Nurkkala, P., *et al.*, 2004. Operational modal analysis of a piping system. *In*: *IMAC XXII conference and exposition on structural dynamics*, 2004 Dearborn. United States: Society for Experimental Mechanics, 2168–2174.

Thomson, W.T. and Dahleh, M.D., 1998. *Theory of vibration with applications*. 5th ed. New Jersey: Prentice Hall.

Wyckaert, K., Augusztinovics, F. and Sas, P., 1996. Vibro-acoustical modal analysis: reciprocity, model symmetry, and model validity. *Journal of the acoustical society of America*, 100 (5), 3172–3181.

Xu, Y., *et al.*, 2014. Frequency modelling and solution of fluid-structure interaction in complex pipelines. *Journal of sound and vibration*, 333, 2800–2822.

Yigang, C., *et al.*, 1987. Experimental modal analysis of metallic pipeline conveying fluid. *In*: *Fifth national congress on pressure vessels and piping*, 1987 San Diego. New York: ASME, 87–90.